Available online at www.sciencedirect.com
SCIENCE DIRECT®
Journal of Computational Physics 191 (2003) 502–524
JOURNAL OF COMPUTATIONAL PHYSICS
www.elsevier.com/locate/jcp

Improved boundary conditions for viscous, reacting, compressible flows

James C. Sutherland [a,*], Christopher A. Kennedy [b]

[a] Department of Chemical and Fuels Engineering University of Utah, Salt Lake City, UT 84112, USA
[b] Combustion Research Facility, Sandia National Laboratories, Livermore, CA 94551, USA

Received 3 December 2002; received in revised form 18 June 2003; accepted 23 June 2003

Abstract

Previous studies on physical boundary conditions for flame–boundary interactions of an ideal, multicomponent, compressible gas have neglected reactive source terms in their boundary condition treatments. By combining analyses of incompletely parabolic systems with those based on the hyperbolic Euler equations, a rational set of boundary conditions is determined to address this shortcoming. Accompanying these conditions is a procedure for implementation into a multidimensional code. In the limits of zero reaction rate or one species, the boundary conditions reduce in a predictable way to cases found in the literature. Application is made to premixed and nonpremixed flames in one and two dimensions to establish efficacy. Inclusion of source terms in boundary conditions derived from characteristic analysis is essential to avoid unphysical generation of pressure and velocity gradients as well as flow reversals. Minor deficiencies in the boundary conditions are attributed primarily to the diffusive terms. Imposing vanishing diffusive boundary-normal flux gradients works better than imposing vanishing fluxes but neither is entirely satisfactory.

Keywords: Reacting flows; Boundary conditions; Navier–Stokes; Characteristic; Flame–boundary interaction

1. Introduction

A recurrent problem encountered during the simulation of compressible fluid flows at open boundaries is how to suppress all unwanted effects of the artificial boundary. The majority of the literature on this topic focuses on boundary conditions derived from the (hyperbolic) Euler equations for a simple gas. There are several different approaches to boundary conditions for the hyperbolic Euler system of equations, (see [1–3] for reviews). Since many of these approaches are designed for use in computational aeroacoustics, they set high standards for the amount of reflection acceptable at outflow boundaries [4].

For viscous, multicomponent, reacting flow fields governed by the (incompletely parabolic) Navier–Stokes equations (NSEs), however, the literature provides far less guidance. In addition to Euler

* Corresponding author.
E-mail address: sutherland@crsim.utah.edu (J.C. Sutherland).

0021-9991/$ - see front matter
doi:10.1016/S0021-9991(03)00328-0

phenomenon (e.g., inviscid wave propagation), physical boundary conditions for reactive NSE flows must consider the possibility of strong diffusive and reactive source terms (e.g. a flame) at or near the boundary. This must be done in a consistent way, and should reduce to an Euler treatment in the absence of diffusive effects [5,6].

Among the most promising approaches to practical and implementable boundary conditions for the NSE are those of Dutt [7] and Hesthaven and Gottlieb [8]. Hesthaven and Gottlieb present asymptotically stable open boundary conditions for the NSE utilizing linearization and localization based on the conservation variables. Their work is rather unique in that it seamlessly combines a characteristic treatment within the incompletely parabolic equation procedure outlined by Gustafsson and Sundström [5]. However, the extension of this approach to gas mixtures remains unsolved. Dutt provides a general approach to reducing the scope of boundary condition possibilities within the structure outlined by Gustafsson and Sundström and Michelson [9]. Poinsot and Lele [10] and Poinsot and Veynante [11] essentially combine the approaches of Dutt for incompletely parabolic systems, with modifications, and Thompson [12] for hyperbolic Euler equations into a particularly useful set of procedures for simple gases. Despite known deficiencies in dealing with acoustic waves which encounter the boundary obliquely [1,2], Thompson's approach is widely used in NSE simulations [10–19].

To our knowledge, Baum et al. [14] and Thévenin et al. [15] offer the only papers which claim to be able to pass a flame through a boundary. As will be shown, these approaches give rise to very large unphysical pressure and velocity waves as flames encounter boundaries. Further, source terms and diffusive terms are neglected in their boundary condition treatment. This paper offers an improvement over these approaches by presenting a unified treatment which allows passage of a flame through the boundary without dramatically affecting the solution on the interior.

The goal of this paper is to provide useful boundary condition strategies that minimize flame–boundary interaction. By clarifying both the number of conditions required and the proper form for these conditions, a well-conceived set of boundary conditions is constructed. The new conditions combine elements from the study of both incompletely parabolic (NSE) and hyperbolic (Euler) equations. A clear approach is then presented to boundary condition specification that allows passage of viscous, exothermic flames through an open inflow or outflow boundary with a minimum of interaction with the boundary. The focus will be on time-accurate simulations as opposed to steady state computations using a Cartesian grid.

In Section 2, general background for incompletely parabolic equations (the multicomponent NSE) such as the proper number and form of the boundary conditions will be considered. Following this, characteristic analysis based on the Euler equations is performed while retaining source terms. Section 3 focuses on the specific form of the subsonic boundary conditions that will be used in this work. These boundary conditions reduce, in a natural way, to those required for nonreacting mixtures as well as those for a single species. Results of applying the proposed boundary conditions to various reacting flow simulations are contained in Section 4. Conclusions are presented in Section 5. Appendix A provides implementation details for characteristic treatment in multidimensional codes.

2. Background

The NSEs for multicomponent reacting flows may be written in terms of the conservative variables $\mathbf{U} = \{\rho u, \rho v, \rho w, \rho, \rho e_0, \rho Y_i\}^{\mathrm{T}}$ as

$$\frac{\partial}{\partial t}\begin{bmatrix}\rho\mathbf{u}_\alpha\\ \rho\\ \rho e_0\\ \rho Y_i\end{bmatrix} = \begin{bmatrix}-\nabla_\beta\cdot(\rho\mathbf{u}_\alpha\mathbf{u}_\beta + p\delta_{\alpha\beta}) + \nabla_\beta\cdot\tau_{\beta\alpha} + \rho\sum_{i=1}^{N} Y_i\mathbf{f}_{i\alpha}\\ -\nabla_\beta\cdot(\rho\mathbf{u}_\beta)\\ -\nabla_\beta\cdot\left[(\rho e_0 + p)\mathbf{u}_\beta\right] + \nabla_\beta\cdot(\tau_{\beta\alpha}\cdot\mathbf{u}_\alpha - \mathbf{q}_\beta) + \rho\sum_{i=1}^{N} Y_i\mathbf{f}_{i\beta}\cdot(\mathbf{u}_\beta + \mathbf{V}_{i\beta})\\ -\nabla_\beta\cdot(\rho Y_i\mathbf{u}_\beta) - \nabla_\beta\cdot(\rho Y_i\mathbf{V}_{i\beta}) + W_i\dot{\omega}_i.\end{bmatrix}, \tag{1}$$

where ∇_β is the gradient operator in direction β, Y_i is the mass fraction of species i, W_i is the molecular weight of species i, $\tau_{\beta\alpha}$ is the viscous stress tensor, $\mathbf{q}_\beta$ is the heat flux vector, $\mathbf{V}_{i\beta}$ is the species mass diffusion velocity, $\dot{\omega}_i$ is the molar production rate of species i, and e_0 is the specific total energy (internal energy plus kinetic energy), $e_0 = (\mathbf{u}_\alpha \cdot \mathbf{u}_\alpha/2) - (p/\rho) + h$. Greek subscripts α, β, and γ are spatial indices, while the subscript i is a species index.

Before one can rationally discuss boundary condition options for the NSE, one must clearly establish: (1) the correct number of boundary conditions that should be applied to assure well-posedness, and (2) the general permissible structure of these conditions. When the proper number of conditions is exceeded, the boundary is over-specified, and two issues arise [6]: (1) it is unclear which boundary conditions are influencing the solution and (2) the underlying solution is generally not continuous. An over-specified boundary may then be regarded as a stationary source of discontinuities [6].

2.1. Number and form of boundary conditions

For simple gases, the appropriate number of boundary conditions for the NSE has been well-established [5,20–23]. Extending the treatment of Gustafsson and Sundström [5] and Strickwerda [20] to multicomponent gases, we obtain Table 1, where N_{dim} is the number of spatial dimensions. $(N-1)$ is used because one species equation is redundant in the presence of the continuity equation.

With the number of boundary conditions to be enforced known, we next consider the proper form of the boundary conditions. Gustafsson and Sundström [5] recommend boundary conditions of the form

$$\begin{pmatrix} \epsilon \mathbf{R}_{11} & 0 \\ 0 & 0 \end{pmatrix} (\mathbf{n} \cdot \nabla) \begin{pmatrix} w_{\text{I}} \\ w_{\text{II}} \end{pmatrix} + \begin{pmatrix} \mathbf{S}_{11} & \mathbf{S}_{12} \\ \mathbf{S}_{21} & \mathbf{S}_{22} \end{pmatrix} \begin{pmatrix} w_{\text{I}} \\ w_{\text{II}} \end{pmatrix} = \mathbf{g}^T, \tag{2}$$

where $\mathbf{n}$ is the boundary-normal direction $\mathbf{g}$ is a prescribed function and ϵ represents a transport coefficient such as viscosity or thermal conductivity. The vector w_{I} represents variables which have diffusive terms in their governing equations, while w_{II} represents variables which do not. For the NSE, $w_{\text{I}} = \{u, v, w, p, Y_i\}$ and $w_{\text{II}} = \{\rho\}$. The choice of p as the energy variable is made for convenience; temperature or entropy is an equally valid choice.

Michelson proves that (2) are uniformly well posed [9]. The goal of this structure is to preclude the formation of strong boundary layers at the computational boundaries [24]. Note that the conditions are essentially Robin-type boundary conditions. Terms having gradients tangential to the boundary are not included in this formulation. Strickwerda [20] includes tangential terms in an analysis that assumes constant viscosity, but gives no suggestions as to implementation. Halpern [21] and Tourrette [25] include tangential terms similar to Strikwerda, but linearize the NSE. The results are cumbersome and their extension to reacting mixtures is a daunting prospect. Another observation on the form of the BCs for the NSE is that terms of the form $(\mathbf{n} \cdot \nabla)(\nabla w)$ (i.e., gradients of fluxes) do not appear to avoid the development of strong boundary layers. This is also consistent with Michelson [9,24]. In spite of this, flux-gradient boundary conditions are often used sucessfully [10,11].

Table 1
Number of boundary conditions required for the Euler and Navier–Stokes Equations

	Euler	Navier–Stokes
Supersonic inflow	$N_{\text{dim}} + 2 + (N-1)$	$N_{\text{dim}} + 2 + (N-1)$
Supersonic outflow	0	$N_{\text{dim}} + 1 + (N-1)$
Subsonic inflow	$N_{\text{dim}} + 1 + (N-1)$	$N_{\text{dim}} + 2 + (N-1)$
Subsonic outflow	1	$N_{\text{dim}} + 1 + (N-1)$

Working within the framework of (2), Dutt [7] provides boundary condition families for supersonic and subsonic outflows and inflows by evaluating a surface integral expressing the time rate-of-change of an entropy-like variable. His results use the thermodynamic fluxes for $\epsilon\mathbf{R}_{11}$. One may extend Dutt's results to gas mixtures in the absence of thermodynamic cross-effects (vanishing thermal diffusion coefficient) for both outflow and inflow cases by considering the minimization of ordinary entropy generation. The resulting form of the boundary conditions is shown in Table 2, where $\mathbf{t}_1$ and $\mathbf{t}_2$ are the boundary-tangential directions, $\mathbf{J}_{i\alpha} = \rho Y_i \mathbf{V}_{i\alpha}$ is the diffusive flux of species i, $\mathbf{q}_{\alpha(\mathrm{red})} = \mathbf{q}_\alpha - \sum_{i=1}^{N} h_i \mathbf{J}_{i\alpha}$ and $\mathbf{q}_\alpha$ are the reduced and ordinary heat flux vectors, h_i is the species specific enthalpy, and α_i and g_i are prescribed functions. Note that these conditions are consistent with Table 1 by reducing to the correct number of conditions in the case of Euler flow. For convenience and because the heat flux and diffusion velocities are treated similarly, we will impose conditions on the ordinary rather than the reduced heat flux vector. Table 2 serves as a general guide for selecting boundary conditions.

Because it is unclear what values to use for α_i and $\mathbf{g}_i$ and there is no obvious way to control boundary reflections, some authors choose to treat convective and diffusive terms separately [10,11] rather than specifying a Robin-type boundary condition. Hesthaven and Gottlieb [8] retain the Robin-type structure. We adopt the approach of treating diffusive and convective terms separately, and use Table 2 as a guideline in combining convective and diffusive boundary conditions.

2.2. Boundary conditions for hyperbolic Euler systems

We now turn our attention to the characteristic treatment of the Euler equations in the hope of combining results with those of the previous analysis. Characteristic treatments offer the possibility of imposing nonreflecting boundary conditions while assuring stability [26]. Thompson [12] presents a unified treatment of characteristic boundary conditions, focusing on the one-dimensional form of the governing equations involving an unsteady term, a scalar source term, and a spatially differentiated term. The analysis considers the equations at three distinct levels: the conservation variables, the primitive variables, and the characteristic variables. The objective is to recast the evolution equations at the conservation and primitive levels in terms found within the evolution equation at the characteristic level. Doing this allows one to operate directly on the characteristics while solving the conservation form of the governing equations. The governing equations may be written at each of the three levels as

$$\frac{\partial \mathbf{U}_a}{\partial t} + \nabla_{(n)} \cdot \mathbf{F}_a^{(\mathrm{n})} + \nabla_{(t)} \cdot \mathbf{F}_a^{(\mathrm{t})} = \mathbf{D}_a^{(\mathrm{n})} + \mathbf{D}_a^{(\mathrm{t})} + \mathbf{s}_a, \tag{3}$$

$$(\mathbf{P})_{ba}^{-1} \Downarrow \quad \Uparrow \mathbf{P}_{ab}$$

$$\frac{\partial \mathsf{U}_b}{\partial t} + \mathsf{A}_{bd}^{(\mathrm{n})} \cdot (\nabla_{(n)} \mathsf{U}_d) + \mathsf{A}_{bd}^{(\mathrm{t})} \cdot (\nabla_{(t)} \mathsf{U}_d) = \mathsf{D}_b^{(\mathrm{n})} + \mathsf{D}_b^{(\mathrm{t})} + \mathsf{s}_b, \tag{4}$$

$$\left(\mathsf{S}^{(\mathrm{n})}\right)_{cb}^{-1} \Downarrow \quad \Uparrow \mathsf{S}_{bc}^{(\mathrm{n})}$$

$$\left(\mathsf{S}^{(\mathrm{n})}\right)_{cb}^{-1} \frac{\partial \mathsf{U}_b}{\partial t} + \mathscr{L}_c^{(\mathrm{n})} + \mathscr{A}_{cd}^{(\mathrm{t})} \cdot (\nabla_{(t)} \mathsf{U}_d) = \mathscr{D}_c^{(\mathrm{n})} + \mathscr{D}_c^{(\mathrm{t})} + \mathfrak{s}_c, \tag{5}$$

where $\mathbf{U}$ and U are the conservation and primitive variables, $\mathbf{D}$, D, and $\mathscr{D}$ are the diffusive terms, $\mathbf{F}$ is related to the convective terms, and $\mathbf{s}$, s, and $\mathfrak{s}$ are source terms. Superscripts (n) and (t) denote the boundary-normal and tangential directions while Roman subscripts a, b, c, d indicate equation indices.

Table 2
Extension of Dutt's subsonic boundary conditions to gas mixtures

	Subsonic outflow	Subsonic inflow
(1)	—	$\rho\mathbf{u}\cdot\mathbf{n} = g_1$
(2)	$(\mathbf{n}\cdot\tau)\cdot\mathbf{n} - \alpha_2(\mathbf{u}\cdot\mathbf{n}) = g_2$	$(\mathbf{n}\cdot\tau)\cdot\mathbf{n} = 0$
(3)	$(\mathbf{n}\cdot\tau)\cdot\mathbf{t}_1 = 0$	$(\mathbf{n}\cdot\tau)\cdot\mathbf{t}_1 - \alpha_3(\mathbf{u}\cdot\mathbf{t}_1) = g_3$
(4)	$(\mathbf{n}\cdot\tau)\cdot\mathbf{t}_2 = 0$	$(\mathbf{n}\cdot\tau)\cdot\mathbf{t}_2 - \alpha_4(\mathbf{u}\cdot\mathbf{t}_2) = g_4$
(5)	$\mathbf{q}_{(\mathrm{red})}\cdot\mathbf{n} = 0$	$\mathbf{q}_{(\mathrm{red})}\cdot\mathbf{n} - \alpha_5 T = g_5$
$(5+i)$	$\rho Y_i(\mathbf{V}_i\cdot\mathbf{n}) = 0,\ i = 1,2,\ldots,N-1$	$\rho Y_i(\mathbf{V}_i\cdot\mathbf{n}) - \alpha_{5+i}Y_i = g_{5+i},\ i = 1,2,\ldots,N-1$

For the analysis done in this paper, $\mathbf{U} = \{\rho u, \rho v, \rho w, \rho, \rho e_0, \rho Y_i\}^{\mathrm{T}}$ and $\mathsf{U} = \{u, v, w, \rho, p, Y_i\}^{\mathrm{T}}$. The choice of pressure as the energy variable is made because of the pressure gradient term in the momentum equations thus keeping the results as clean as possible. It is equally correct, although far more messy, to choose temperature or entropy as the energy variable. The matrices in (3)–(5) are given by $\mathsf{A} = \mathbf{P}^{-1}\mathbf{Q}$, $\mathbf{Q} = \partial\mathbf{F}/\partial\mathsf{U}$, $\mathbf{P} = \partial\mathbf{U}/\partial\mathsf{U}$, and the columns of $\mathsf{S}^{(\mathrm{n})}$ are the right eigenvectors of $\mathsf{A}^{(\mathrm{n})}$. Expressions for $\mathbf{P}$ and $\mathbf{Q}$ are given in Appendix A. Comparing (1) and (3), one may easily determine $\mathbf{F}$, $\mathbf{D}$, and $\mathbf{s}_a$. Then, the terms in Eqs. (4) and (5) may be determined using the matrices $\mathbf{P}$ and S.

For characteristic boundary treatments, viscous/diffusive terms are dropped and only boundary-normal inviscid terms are retained, leading to the locally one-dimensional inviscid (LODI) equations, which may be written terms of conserved, primitive, and characteristic variables as

$$\frac{\partial \mathsf{U}_a}{\partial t} + \mathbf{P}_{ab}\mathsf{S}^{(\mathrm{n})}_{bc}\mathscr{L}^{(\mathrm{n})}_c = \mathbf{s}_a, \quad \frac{\partial \mathsf{U}_b}{\partial t} + \mathsf{S}^{(\mathrm{n})}_{bc}\mathscr{L}^{(\mathrm{n})}_c = \mathsf{s}_b, \quad \left(\mathsf{S}^{(\mathrm{n})}\right)^{-1}_{cb}\frac{\partial \mathsf{U}_b}{\partial t} + \mathscr{L}^{(\mathrm{n})}_c = \mathfrak{s}_c, \tag{6}$$

where sometimes one defines $\mathsf{d}^{(\mathrm{n})}_b = \mathsf{S}^{(\mathrm{n})}_{bc}\mathscr{L}^{(\mathrm{n})}_c$. The $\mathscr{L}^{(\mathrm{n})}_c$ are the wave amplitudes for the characteristic variables. Thus, by controlling the $\mathscr{L}_c$, we are able to directly control waves propagating through the domain. Hedstrom's [27] criterion for nonreflection now becomes $\mathscr{L}^{(\mathrm{n})}_c = \mathfrak{s}_c$, rather than $\mathscr{L}^{(\mathrm{n})}_c = 0$ as is commonly done.

The specific values of $\mathbf{P}_{ab}\mathsf{S}^{(\mathrm{n})}_{bc}\mathscr{L}^{(\mathrm{n})}_c$, $\mathsf{S}^{(\mathrm{n})}_{bc}\mathscr{L}^{(\mathrm{n})}_c$, $(\mathsf{S}^{(\mathrm{n})})^{-1}_{cb}\partial\mathsf{U}_b/\partial t$, and $\mathscr{L}^{(\mathrm{n})}_c$ for each boundary-normal direction as well as s_b and $\mathfrak{s}_c$ are given in Appendix A.

3. Boundary closures

Having now established the form and number of boundary conditions for the NSE, we now consider specific boundary conditions and their implementation within the framework established in Sections 2.1 and 2.2.

3.1. Subsonic nonreflecting outflow conditions

For a subsonic outflow, Table 1 shows that the Euler equations require 1 condition while the Navier–Stokes require $(4+N-1)$. All eigenvalues of $\mathsf{A}^{(\mathrm{n})}$ are leaving the domain except one. At the left end of the domain, $\lambda_5 = u + c$ is entering the domain while at the right end, $\lambda_1 = u - c$ is entering. Smooth transition from Navier–Stokes boundary conditions to Euler boundary conditions suggests that we should use only $(3+N-1)$ viscous boundary conditions (as they vanish in the Euler limit). From Table 2, we may set $(\mathbf{n}\cdot\tau)\cdot\mathbf{t}_1 = 0$, $(\mathbf{n}\cdot\tau)\cdot\mathbf{t}_2 = 0$, $\mathbf{q}\cdot\mathbf{n} = 0$, $(\rho Y_i\mathbf{V}_i)\cdot\mathbf{n} = 0$. However, we found that specifying zero fluxes normal to the boundary was unstable. This is not surprising, given that this would introduce strong spatial discontinuities into the diffusive fluxes which, when differentiated, would produce very large terms in the governing equations. When nothing is known a priori about the flux profile, it may be prudent to impose a

vanishing boundary-normal flux gradient. This is also not ideal, and violates the structure shown in (2), but it is also not as severe as zeroing the boundary-normal flux. Poinsot and Lele and Poinsot and Veynante choose this approach by imposing a slight variation of what Dutt proposed:

$$(\nabla_\gamma \tau_{\beta\alpha})\mathbf{n}_\gamma \mathbf{n}_\beta \mathbf{t}_{1,\alpha} = 0, \quad (\nabla_\gamma \tau_{\beta\alpha})\mathbf{n}_\gamma \mathbf{n}_\beta \mathbf{t}_{2,\alpha} = 0, \quad (\nabla_\beta \mathbf{q}_\alpha)\mathbf{n}_\beta \mathbf{n}_\alpha = 0, \quad [\nabla_\beta(\rho Y_i \mathbf{V}_{i\alpha})]\mathbf{n}_\beta \mathbf{n}_\alpha = 0. \tag{7}$$

As the dimensionality of the problem is reduced, the tangential conditions in (7) dissolve. Imposing the vanishing of still higher boundary-normal gradients (which is an even stronger violation of (2)) does not work. Alternatively, if one were to keep track of fluxes as they approached the outflow boundary, it might be possible to reasonably specify the fluxes as nonzero rather than having to resort to imposing flux gradients. This may be useful if tangential fluxes are small [28]. We should point out that Nordström [29] found that imposing second-derivative conditions at a supersonic boundary gave rise to time-exponential error growth at the boundary. He also comments that one cannot expect accurate results through imposition of vanishing second-derivatives at an subsonic outflow boundary [30]. Furthermore, as mentioned in Section 2.1, there is no theoretical justification for specifying second derivative conditions. However, while many boundary condition formulations do not lead to a well-posed problem (as may be the case with (7)), they may produce good results when applied to practical problems [31].

The last boundary condition that we may specify without over-prescribing the boundary should be either inviscid or a Robin boundary condition having inviscid and viscous parts. This way one boundary condition is imposed regardless of whether the flow is Euler or Navier–Stokes. As it is unclear how to apply Dutt's boundary-normal momentum condition rationally, we instead choose a characteristic condition. This allows us to use the last degree of freedom to minimize reflection. Therefore, we wish to control $\mathscr{L}_5$ at the left end of the domain (because $\lambda_5 = u + c$ is entering) and $\mathscr{L}_1$ at the right end. Extending the treatment of Rudy and Strikwerda [32] and Poinsot and Lele to include source terms, we set

$$\mathscr{L}_5 = \mathfrak{s}_5 + [\sigma c(1 - \mathscr{M}^2)(p - p_\infty)]/2L, \quad \text{Left Boundary}, \tag{8}$$

$$\mathscr{L}_1 = \mathfrak{s}_1 + [\sigma c(1 - \mathscr{M}^2)(p - p_\infty)]/2L, \quad \text{Right Boundary}, \tag{9}$$

where Rudy and Strikwerda suggest $\sigma = 0.287$, c is the speed of sound, $\mathscr{M}$ is a suitable Mach number associated with the boundary, p is the pressure at the boundary point, p_∞ is some reference pressure we would like the boundary to stay near, and L is the length of the computational domain normal to the boundary. The source terms $\mathfrak{s}_1$ and $\mathfrak{s}_5$ are nonzero and given in Table 4.

In summary, for a nonreflecting outflow condition, we impose viscous conditions according to (7) and characteristic equations according to (8) and (9).

3.2. Subsonic inflow conditions

For a subsonic inflow, Table 1 shows that the Euler equations require $(4 + N - 1)$ conditions whereas the Navier–Stokes require $(5 + N - 1)$. A seamless transition from Navier–Stokes to Euler conditions suggests that one of these conditions should be purely viscous. Diffusive and heat fluxes are each vector quantities and share the same thermodynamic forces. It does not make sense to arbitrarily manipulate one of these alone. Viscous stress has two tangential components and one normal component. Hence, if only one flux term must be manipulated, normal stress would seem most reasonable. Dutt recommends $(\mathbf{n} \cdot \tau) \cdot \mathbf{n} = 0$ to achieve a maximally dissipative boundary condition. Poinsot and Lele recommend a slight adaptation of this;

$$(\nabla_\gamma \tau_{\beta\alpha})\mathbf{n}_\gamma \mathbf{n}_\beta \mathbf{n}_\alpha = 0. \tag{10}$$

If inflow data permits and it is sufficiently equilibrated, one might be well advised to impose the actual value of $(\mathbf{n}\cdot\tau)\cdot\mathbf{n}$. With the viscous condition specified using one of these three options, we have $(4+N-1)$ conditions remaining. We now discuss two ways to impose these conditions.

3.2.1. Nonreflecting inflow conditions

Nonreflecting boundary conditions are achieved by setting as many $\mathscr{L}_a = \mathfrak{s}_a$ as possible. Therefore, we achieve a nonreflecting inflow by setting

$$\mathscr{L}_2 = \mathfrak{s}_2, \quad \mathscr{L}_3 = \mathfrak{s}_3, \quad \mathscr{L}_4 = \mathfrak{s}_4, \quad \mathscr{L}_{5+i} = \mathfrak{s}_{5+i}. \tag{11}$$

On the left boundary, $\mathscr{L}_5 = \mathfrak{s}_5$ is set, while on the right boundary, this is reversed, and $\mathscr{L}_1 = \mathfrak{s}_1$ is set. Eqs. (10) and (11), along with a condition on $\mathscr{L}_5$ or $\mathscr{L}_1$ on the right and left boundaries, respectively, provide a complete specification of a nonreflecting inflow.

It should be remarked that several papers make a subtle over-specification on certain boundaries. For a subsonic inflow where one would like to specify many of the variables directly, Poinsot and Veynante [11] offer a subsonic inflow (which they call SI-1) where they are permitted $5+(N-1)$ conditions. They specify u, v, w, T, and $(N-1)$ of the Y_i. One condition is then available for specification. They then impose conditions on d_1, along with $\mathscr{L}_3 = 0$, $\mathscr{L}_4 = 0$, and $\mathscr{L}_{5+i} = 0$. Although it is true that these last three conditions are consequences of their LODI system rather than independent specifications, this is not true for the equations to which the conditions are actually being applied, the NSE. Hence they are specifying $7+2(N-1)$ conditions. It is likely that this over-specification is mild because of the, hopefully, minor deviation between the one-dimensional Euler and multidimensional NSE at the boundary grid points.

3.2.2. Hard inflow conditions

At a hard inflow, we wish to directly specify many of the variables in, possibly, a time dependent manner. At the same time we would like that the inflow boundary not be a strong source of disturbances. One may also ask the hard inflow boundary to be relatively transparent to waves emanating from within the computation domain [18]. Simultaneously doing each of these at the inflow of a reacting fluid is a tall order. We therefore attempt to specify a reacting flow which minimizes the disturbance output of the boundary. There are many approaches to this matter. One is to simply specify $\{u, v, w, T, Y_i\}$ along with a condition on the boundary-normal viscous stress associated with the boundary-normal momentum equation, as described in (10).

Poinsot and Lele also propose, in the context of a simple gas, a condition where effectively $\{u, v, w, T, Y_i\}$ are specified but a nonviscous condition replaces the viscous condition described above. If the flow should be locally Euler flow, however, the boundary would become over-specified. With this caveat, we look for a time dependent LODI relation for either pressure or density; $\partial \mathsf{U}_a/\partial t + \mathsf{d}_a^{(\mathrm{n})} = \mathsf{s}_a$ in order to keep the perturbations introduced into each variable self-consistent to the one-dimensional Euler level. The equation of state will allow the other to be determined as temperature and mass fraction have already been specified. Choosing density, $\mathsf{d}_1^{(\mathrm{n})}$ is a function of $\mathscr{L}_1$, $\mathscr{L}_2$, and $\mathscr{L}_5$. For pressure, $\mathsf{d}_2^{(\mathrm{n})}$ is a function of $\mathscr{L}_1$, and $\mathscr{L}_5$. We choose the former because it allows the incorporation of more degrees of unsteadiness than the latter as well as the fact that this approach has met with prior success [10,14]. We first write

$$\frac{\partial \rho}{\partial t} + \mathsf{d}_1^{(\mathrm{n})} = \frac{\partial \rho}{\partial t} + \frac{1}{c^2}\left[c^2\mathscr{L}_2^{(\mathrm{n})} + \left(\mathscr{L}_5^{(\mathrm{n})} + \mathscr{L}_1^{(\mathrm{n})}\right)\right] = 0. \tag{12}$$

At the left boundary, $\mathscr{L}_1$ is imposed from interior data while $\mathscr{L}_2$ and $\mathscr{L}_5$ are chosen. At the right boundary, $\mathscr{L}_5$ is imposed from interior data while $\mathscr{L}_2$ and $\mathscr{L}_1$ are chosen. Let us assume that each imposed variable includes time variation as $\mathbf{u}\cdot\mathbf{n} = u = \mathsf{u}(t)$, $T = \mathsf{T}(t)$, and $Y_i = \mathsf{Y}_i(t)$. Therefore,

$$\frac{\partial \mathsf{u}}{\partial t}+\frac{1}{\rho c}\left(\mathscr{L}_5^{(\mathrm{n})}-\mathscr{L}_1^{(\mathrm{n})}\right)=\mathsf{s}_u, \tag{13}$$

$$\frac{\partial \mathsf{T}}{\partial t}+\frac{p\mathsf{d}_2^{(\mathrm{n})}}{T}-\frac{T\mathsf{d}_1^{(\mathrm{n})}}{\rho}-T\sum_{i=1}^{N-1}W_{iN}\mathscr{L}_{5+i}^{(\mathrm{n})}=\frac{T}{p}\mathsf{s}_p-T\sum_{i=1}^{N-1}W_{iN}\mathsf{s}_{Y_i}, \tag{14}$$

$$\frac{\partial \mathsf{Y}_i}{\partial t}+\mathscr{L}_{5+i}^{(\mathrm{n})}=\mathsf{s}_{Y_i}, \tag{15}$$

where $W_{iN}=W(W_i^{-1}-W_N^{-1})$, W is the mixture molecular weight, and $\mathsf{d}_1^{(\mathrm{n})}$ and $\mathsf{d}_2^{(\mathrm{n})}$ are given in Table 7. Solving these equations, we now specify either $\mathscr{L}_1$ or $\mathscr{L}_5$ from interior data and use

$$\mathscr{L}_5^{(\mathrm{n})}=\mathscr{L}_1^{(\mathrm{n})}-\rho c\left(\frac{\partial \mathsf{u}}{\partial t}-\mathsf{s}_u\right),\quad \mathscr{L}_1^{(\mathrm{n})}=\mathscr{L}_5^{(\mathrm{n})}+\rho c\left(\frac{\partial \mathsf{u}}{\partial t}-\mathsf{s}_u\right), \tag{16}$$

$$\mathscr{L}_2^{(\mathrm{n})}=\frac{(\gamma-1)}{c^2}\left(\mathscr{L}_5^{(\mathrm{n})}+\mathscr{L}_1^{(\mathrm{n})}\right)+\frac{\rho}{T}\frac{\partial \mathsf{T}}{\partial t}+\rho W\sum_{i=1}^{N-1}\left(W_{iN}\frac{\partial \mathsf{Y}_i}{\partial t}\right)-\frac{\rho}{p}\mathsf{s}_p, \tag{17}$$

to complete the specification of $\mathsf{d}_1^{(\mathrm{n})}$ in (12).

3.3. Implementation strategy

Implementation of boundary conditions such as those described above is problematic. Ultimately, boundary conditions need to be specified on the integration vector of conservation variables, **U**. However, actual boundary conditions at hand may appear on primitive variables like temperature or other variables that are nontrivially related to the conservation variables such as entropy. Further, boundary conditions may involve linear combinations of all of these variables and their gradients or contain transport coefficients with complicated functional dependencies. To avoid internal inconsistency, one must establish a procedure whereby any arbitrary set of boundary conditions may be uniquely and accurately mapped onto specifications of **U**. Computationally, this should be an expeditious procedure. As this is a daunting challenge, we choose to accept some degree of internal inconsistency in the interest of ease of implementation. We make no claim of internal consistency or that the following procedure is best. With these caveats, our implementation procedure is as follows.

(1) At the beginning of all stages or steps of the time-integration, decompose the **U**-vector into needed primitive variables, $\mathsf{U}=\{u,v,w,\rho,p,Y_i\}$.
(2) Impose any boundary conditions involving primitive variables.
(3) Compute diffusive flux terms ($\tau_{\beta\alpha}$, $\mathbf{q}_\alpha$, $\rho Y_i\mathbf{V}_{i\alpha}$).
(4) Impose any boundary conditions on the diffusive flux terms.
(5) Compute the full right-hand side (RHS) of all equations.
(6) Impose characteristic boundary conditions as required. This is done in two steps. First, we remove the terms in the RHS associated with the characteristics, $\nabla_{(n)}\cdot\mathbf{F}^{(\mathrm{n})}$ at all boundary points.
   (a) Using Table 5, compute all $\mathscr{L}_a^{(n)}$ from *interior data*. This is done independent of whether the associated eigenvalue is entering or leaving the domain.
   (b) Using Table 7, compute $\mathsf{d}_b^{(n)}$ from $\mathscr{L}_a^{(n)}$.
   (c) Using Table 8, compute $\nabla_n\cdot\mathbf{F}^{(\mathrm{n})}$ from the $\mathsf{d}_b^{(n)}$ and subtract it from each RHS.

Second, we impose characteristic boundary conditions by manipulating the $\mathscr{L}_a^{(n)}$, update $\nabla_{(n)}\cdot\mathbf{F}^{(\mathrm{n})}$ at all boundary points, and then add it back to the RHS.

(a) Impose values for $\mathscr{L}_a^{(n)}$ associated with incoming eigenvalues according to the physical boundary conditions. The $\mathscr{L}_a^{(n)}$ associated with outgoing eigenvalues are computed from interior data using Table 5.
(b) Using Table 7, recompute the $\mathrm{d}_b^{(n)}$ from the $\mathscr{L}_a^{(n)}$ (some of which were modified in the previous step).
(c) Using Table 8, compute $\nabla_{(n)} \cdot \mathbf{F}^{(\mathrm{n})}$ from the revised $\mathrm{d}_b^{(n)}$ and add it back to each RHS.

(7) Update the **U**-vector at all boundary points using the corrected RHS.

4. Results

Numerical experiments to test the proposed boundary conditions are done using a three-dimensional Direct Numerical Simulation (DNS) code. The code solves the compressible, multicomponent, reacting Navier–Stokes in conservation form as given by (1). Supplementary relations that are needed to solve this system are given in many books [33]. Body force terms, barodiffusion, and terms involving the thermal diffusion coefficient are neglected. Mixture-averaged transport coefficients are calculated from the CHEMKIN TRANSPORT package [34]. For the results presented here, we used a hydrogen–air mechanism developed by Yetter et al. [35]. Since body forces such as gravity are not considered, the only nonzero source terms in (6) are s_p and s_{Y_i}. From the results given in Appendix A, we may write s_p and s_{Y_i} as

$$\mathsf{s}_p = \rho(1-\gamma)\sum_{i=1}^{N-1}(\mathfrak{h}_i - \mathfrak{h}_N)\mathsf{s}_{Y_i}, \quad \mathsf{s}_{Y_i} = W_i\dot{\omega}_i/\rho. \tag{18}$$

The corresponding sources at the characteristic level, $\mathfrak{s}_c$, may be determined from Table 4.

The governing equations are discretized in space on a rectangular Cartesian grid using eighth-order, explicit finite-difference derivatives. Boundary closures to the derivative operators are $(3,3,4,6-8-6,4,3,3)$ [36]. Although Rowley and Colonius [4] study the effects of lower-order numerical boundary stencils for derivative operators on boundary condition behavior, this matter seems quite secondary for flame–boundary interactions. Tenth-order filtering is done on the conservation variables at each step to remove unresolved wavenumber information [36]. Time integration is accomplished using a six-stage, fourth-order vdH-type, low-storage Runge–Kutta method in conjunction with a PID error controller [37]. The Runge–Kutta pair is SC-stable at all points along its stability boundary.

Here and below, we will distinguish between two different nonreflecting outflow boundary conditions: A and B. Nonreflecting A disregards source terms by setting $\mathfrak{s}_c = 0$, and, with the exception of the diffusive treatment, is equivalent to the conditions suggested by Baum et al. [14]. Nonreflecting B retains source terms, with $\mathfrak{s}_c$ given in Table 4.

4.1. Comments on nonreflecting inflow conditions

As mentioned in Section 3.2.1, one condition at a nonreflecting inflow is $\mathscr{L}_{5+i} = \mathfrak{s}_{5+i}$. It should be mentioned that at a nonreflecting inflow, the source terms in the species equations at the characteristic level, $\mathfrak{s}_{5+i} = \mathsf{s}_{Y_i}$ should be neglected, i.e., set $\mathscr{L}_{5+i} = 0$. We have found that including source terms in the characteristic species equations can lead to unstable results regardless of the stiffness of the chemical mechanism. For example, feeding a stoichiometric premixture of hydrogen and air at 500 K yielded time-unstable boundary behavior for $\mathscr{L}_{5+i} = \mathfrak{s}_{5+i}$. If $\mathscr{L}_{5+i} = 0$ was used, however, there was no problem. While the characteristic species equations are not stable when source terms are included, the term s_p is not a problem since it involves a summation over the heats of reaction, which seems to be less destabilizing than individual reaction rates. All results presented below will use $\mathscr{L}_{5+i} = 0$ at nonreflecting inflows.

4.2. Case 1: 1D premixed ignition

For this case, a stoichiometric mixture of hydrogen and air is ignited by a temperature spike. The domain is 2.0 mm with $\Delta x = 10$ μm, and the average timestep was near 1×10^{-8} s. The domain initially contains a stoichiometric premixture of H_2 and air at 300 K and 1 atm pressure. There is no mean convective velocity imposed. A gaussian temperature spike is placed in the mixture at $x = 1.2$ mm to provide an ignition source. The spark is placed off center in the domain to eliminate symmetry and allow the flame fronts to encounter the boundaries at different times. Both left and right boundaries are non-reflecting (see

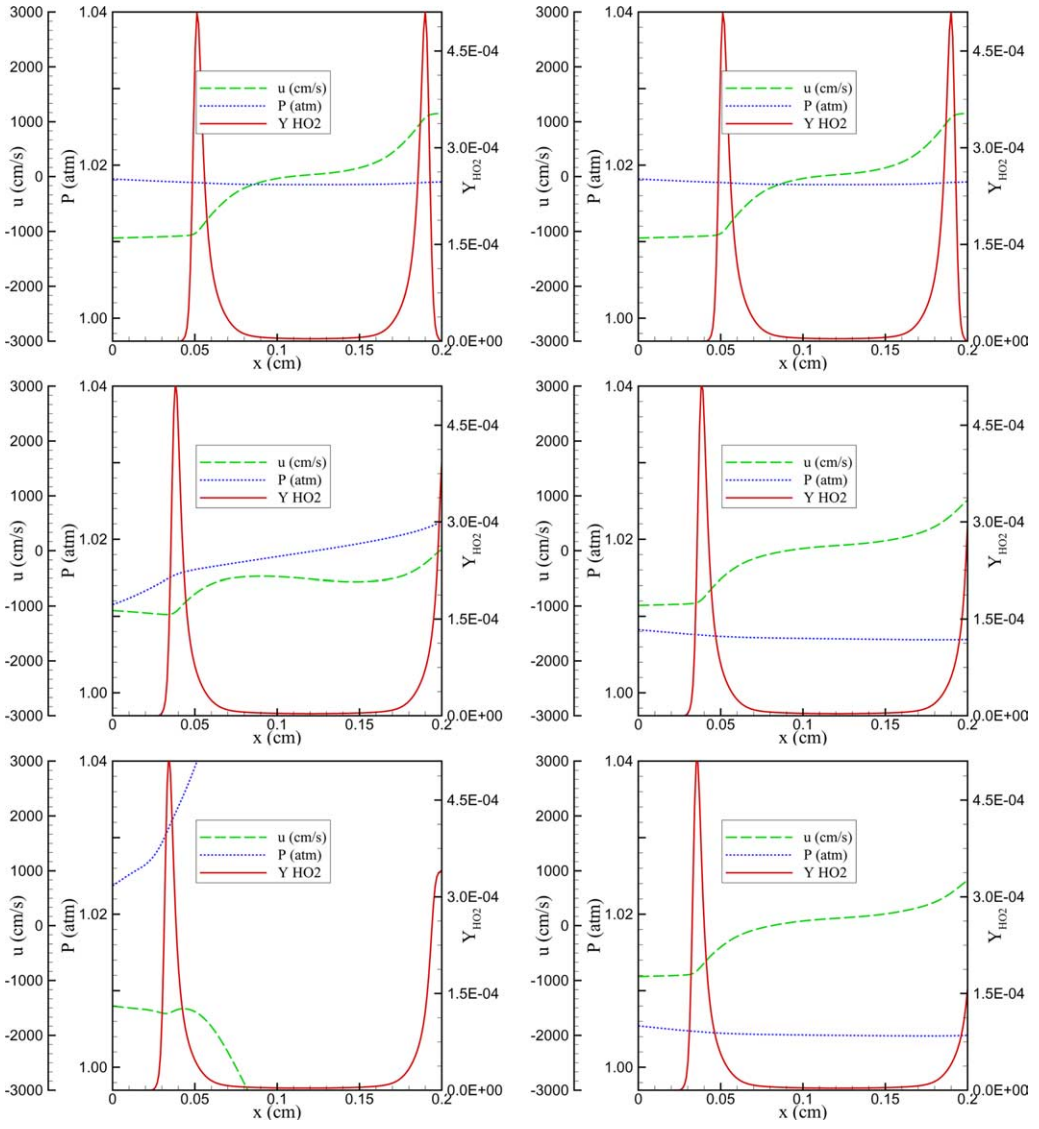

Fig. 1. Velocity (dashed) and Pressure (dotted) fields for Case 1 at 3.0, 4.0, and 4.25×10^{-5} s. HO_2 mass fraction (solid) is shown to indicate flame position. Both boundaries are nonreflecting. The figures on the left use nonreflecting A; figures on the right use nonreflecting B.

Section 3.1), and the diffusive conditions applied at both boundaries are $\partial \mathbf{q}_x/\partial x = 0$, $\partial \mathbf{J}_{x,i}/\partial x = 0$, $i = 1, 2, \ldots, N-1$.

As time proceeds, we expect to see a pressure rise associated with ignition, and then the pressure should equilibrate back to 1 atm. Two premixed flame fronts will develop and propagate outward toward the nonreflecting boundaries, generating an outward convective velocity due to the expansion associated with combustion. Ideally, the boundary conditions should have no effect on any of the solution variables. Fig. 1 shows the velocity and pressure profiles at various times for nonreflecting A (which neglects source terms) and nonreflecting B (which retains source terms) in the left and right columns, respectively. The mass fraction of HO_2 is also shown to indicate the flame position. The first frame in Fig. 1 is shown after the initial pressure and velocity waves associated with ignition have exited the domain. Both approaches are identical until the flame encounters the boundary, at which point nonreflecting A gives rise to large pressure and velocity waves which are generated at the boundary and propagate back through the domain. The second frame in Fig. 1 shows that nonreflecting A has developed a large pressure gradient. Indeed, the pressure gradient is so strong that a flow reversal is generated by nonreflecting A, as shown in the second and third frames. The pressure gradient in the third frame is enormous, as is the velocity. Note from the first frame that the maximum velocity is near 11 m/s. However, the velocity induced by nonreflecting A is approximately 44 m/s in the $(-x)$ direction. It is clear from Fig. 1 that nonreflecting A (which ignores source terms in the analysis) completely fails when the flame encounters the boundary. On the other hand, nonreflecting B (which retains source terms in the analysis) performs quite satisfactorily.

4.3. Case 2: 1D nonpremixed ignition with convective flow

Baum et al. [14] demonstrated a nonpremixed flame with a hard inflow left boundary and a nonreflecting outflow condition on the other end of the domain. A similar configuration is considered here, where the left boundary is a hard-inflow (see Section 3.2.2) and the right boundary is nonreflecting (see Section 3.1). Viscous conditions at the right (outflow) boundary are $\partial \mathbf{q}_x/\partial x = 0$, $\partial \mathbf{J}_{x,i}/\partial x = 0$, $i = 1, 2, \ldots, N-1$. At the left (inflow) boundary, $\partial \tau_{xx}/\partial x = 0$ is applied for the viscous condition. The domain is 7.0 mm in length, with a grid spacing of 10 μm and a timestep of 1.5×10^{-8} s. The fuel is 50% H_2 and 50% N_2 at 300 K, and the oxidizer is air at 1300 K. A plot of the initial H_2, O_2, and temperature profiles is shown in Fig. 2. The initial velocity throughout the domain is 13.0 m/s. The inlet velocity is held fixed at 13.0 m/s, and the inlet temperature and composition are that of the fuel. As time proceeds, ignition occurs near the stoichiometric mixture fraction, and a flame develops. The domain considered here is longer than that considered by Baum et al. to allow the flame more time to develop before it encounters the boundary.

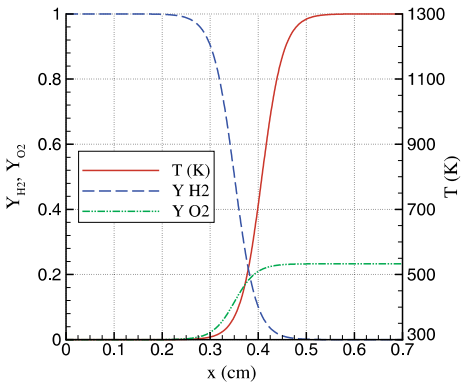

Fig. 2. Initial condition for Case 2 condition showing H_2, O_2, and temperature profiles.

Fig. 3 shows the evolution of pressure and velocity profiles. The left column uses nonreflecting A and the right column uses nonreflecting B. The first frame in Fig. 3 shows the initial conditions. The second frame shows the field after ignition, at which point nonreflecting A and B are indistinguishable. As the flame encounters the boundary, however, we observe a large pressure rise from nonreflecting A, while the pressure in nonreflecting B is equilibrating with the surroundings, and remains unaffected by the flame encountering the boundary. The magnitude of the pressure rise in nonreflecting A when the flame encounters the boundary is larger than the pressure rise associated with ignition!

While nonreflecting A demonstrates unphysical behavior in the pressure and velocity fields as the flame passes through the boundary, the hard inflow boundary acts to limit the magnitude and duration of the disruptions by maintaining a fixed velocity at the left boundary. While the failure of nonreflecting A is much less pronounced in this case, it is still present, and is not at all negligible.

It is worthwhile to note that if a nonreflecting inflow condition were used rather than a hard inflow at the left boundary, then the failure of nonreflecting A becomes much more evident. At a nonreflecting boundary, the velocity and composition are *not* held fixed. Fig. 4 shows results at 1.0 and 1.6×10^{-4} s. Initial conditions are identical to those described previously. At 1.0×10^{-4} s, we see that the species profiles are identical. However, there are discernable differences in the pressure and velocity fields. The pressure at the right boundary is higher for nonreflecting A than for nonreflecting B. This is due to the flame interacting with the boundary. As time proceeds, nonreflecting A generates a huge pressure gradient and a flow reversal, while nonreflecting B remains stable and allows the flame to pass without disruption on the pressure or velocity fields. Comparing Figs. 3 and 4, we see that the hard inflow masks the failure of nonreflecting A in Fig. 3.

4.4. Case 3: 2D premixed flame

Demonstrating the performance of boundary conditions in one-dimensional configurations is useful, but most practical applications of these boundary conditions are to multidimensional flows. Case 3 considers a two-dimensional premixed flame front propagating through nonreflecting boundaries. All four boundaries are nonreflecting (see Section 3.1), with viscous conditions at x boundaries $\partial \mathbf{q}_x/\partial x = 0$, $\partial \mathbf{J}_{x,i}/\partial x = 0$, $i = 1, 2, \ldots, N-1$, $\partial \tau_{xy}/\partial x = 0$, and at y boundaries $\partial \mathbf{q}_y/\partial y = 0$, $\partial \mathbf{J}_{y,i}/\partial y = 0$, $i = 1, 2, \ldots, N-1$, $\partial \tau_{yx}/\partial y = 0$. The domain is 2.0 mm $\times$ 2.0 mm, with 150 points in each direction, and initially contains a stoichiometric premixture of H_2 and O_2 at 300 K and 1 atm pressure, with a gaussian temperature spike centered at $x = y = 1.2$ mm. The premixture ignites and a premixed flame front propagates outward toward the boundaries.

Fig. 5 shows pressure contours at 1.0, 4.0, 5.5, and 8.5×10^{-5} s, with the mass fraction HO_2 superimposed to mark the flame position. As time proceeds, nonreflecting B remains stable, while nonreflecting A gives completely unphysical results. The first frame in Fig. 5 shows that, before the flame hits the boundary, the two simulations are identical. The second frame shows the fields as the flame hits the boundary. The pressure field for nonreflecting A shows a significant pressure gradient developing. In the third frame in Fig. 5 nonreflecting A generates a flow reversal at the top and right boundaries, indicated by the HO_2 contours. The pressure field for nonreflecting A is highly disrupted relative to the pressure field for nonreflecting B, and contains large pressure gradients. At 8.5×10^{-5} s (the fourth frame), nonreflecting B still shows the flame structure approaching the left and bottom boundaries with the pressure field uniform at 1 atm (unchanged from the initial condition). Nonreflecting A, on the other hand, shows that the flame has been obliterated, with flame fragments remaining in the upper left, upper right, and lower right corners. The pressure field is also highly disrupted, with very large pressure gradients in the domain. Furthermore, the maximum velocity (not shown here) for nonreflecting A at 85 μs is nearly 32 m/s, an order of magnitude larger than the velocities in the domain prior to the flame hitting the boundary. The behavior exhibited by nonreflecting A is completely unphysical.

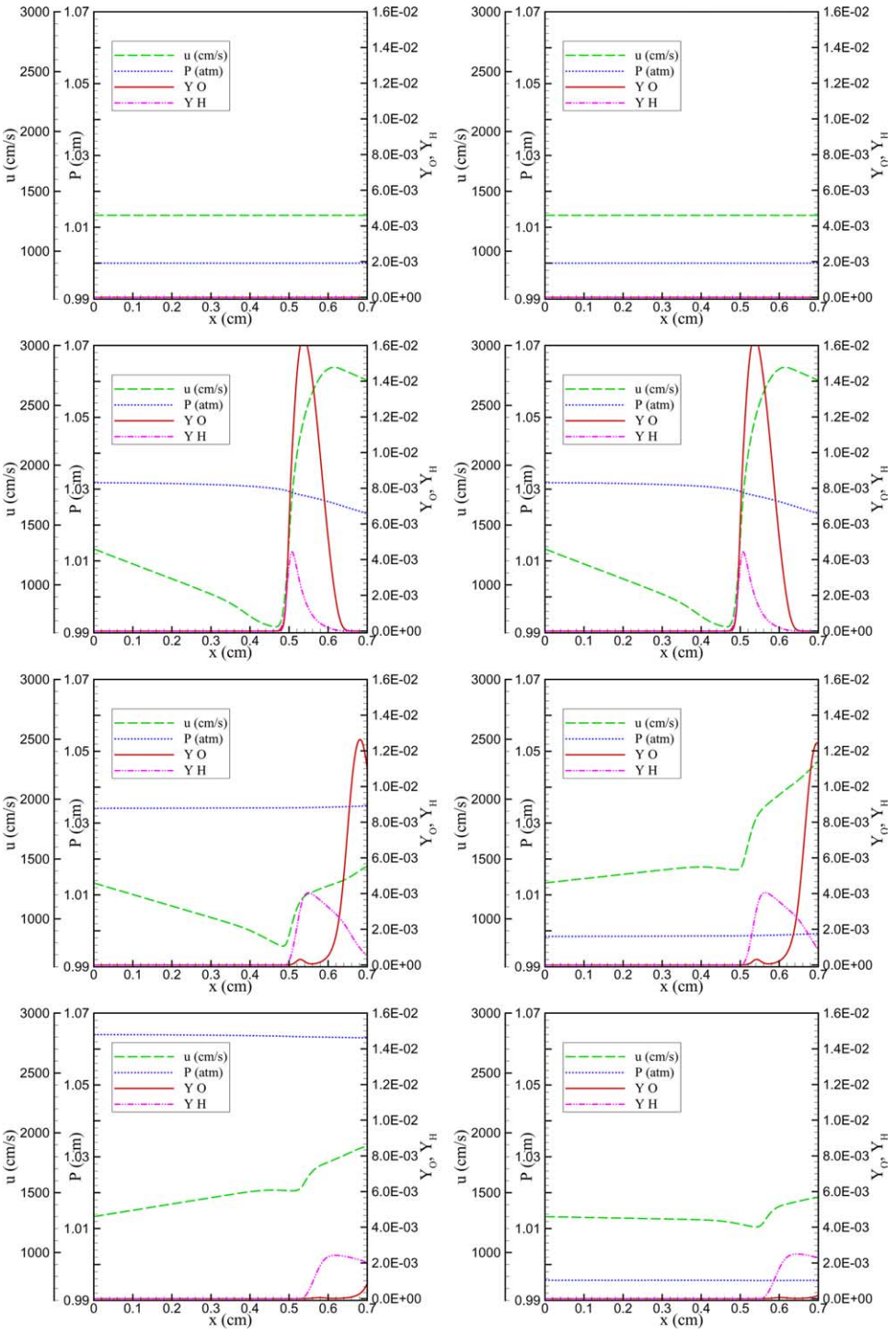

Fig. 3. Results for Case 2 at 0.0, 0.6, 1.1 and 1.6×10^{-4} s. Left boundary is hard inflow, right boundary is nonreflecting. The figures on the left use nonreflecting A; figures on the right use nonreflecting B.

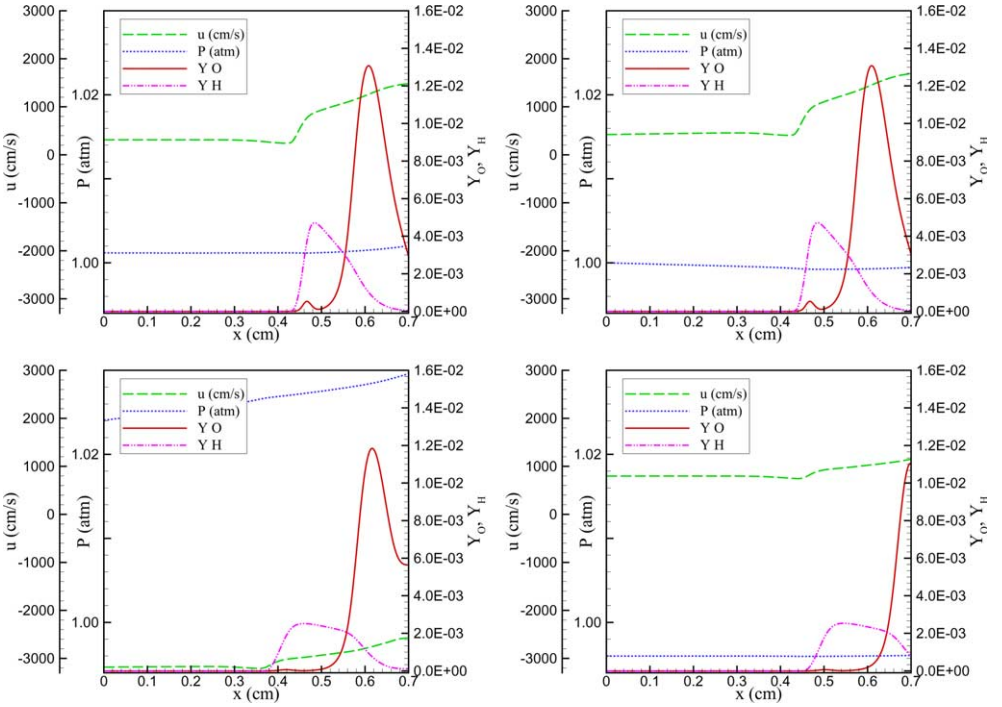

Fig. 4. Pressure and velocity profiles for Case 2 at 1.0 and 1.6×10^{-4} s. Both boundaries are nonreflecting. The figures on the left use nonreflecting A; figures on the right use nonreflecting B. Note that the velocity scale is different from Fig. 3.

Fig. 5 also demonstrates a few deficiencies in the boundary conditions that were not observed in the one-dimensional cases. The first noticeable shortcoming is in the pressure field. The pressure contours should be circular and concentric with the flame. Note that for both nonreflecting A and B, the pressure field is *not* circular, even at 1.0×10^{-5} s, when the flame has not yet encountered the boundary. Earlier in the simulation, acoustic waves are generated from the temperature spike in the initial condition and these waves propagate outward, encountering the boundaries at different angles and at different times. Slight deficiencies in the boundary conditions are manifested by the pressure field losing its circular character and becoming more square-shaped, as seen in Fig. 5 at 3 μs. These deficiencies in characteristic-based boundary conditions are attributable to partial reflection of oblique waves and are well-known [1,2]. The contributions made herein do not address this shortcoming of the boundary conditions. However, these deficiencies are quite secondary in comparison to the deficiencies in former boundary treatments (nonreflecting A) as a flame encounters the boundary.

The second shortcoming of the boundary conditions is that as the flame approaches an outflow boundary, it accelerates slightly. This can be seen by examination of the HO_2 field, in frames 2–4 of Fig. 5. This distortion occurs with both nonreflecting A (before failure) and nonreflecting B, and appears to be due to the treatment of the diffusive terms. As discussed in Section 3.1 we apply a zero normal flux gradient condition at these boundaries. In a flame, both the diffusive flux *and* its gradient may be large. Thus, specifying zero boundary-normal fluxes or zero boundary-normal flux gradients is not physically realistic. Fig. 6 shows the heat flux contours and vectors at various times as the flame encounters the boundary. Clearly, the specification of zero flux gradient for heat fluxes at the boundary over-predicts the heat flux as the flame approaches the boundary. The same is true for the diffusive flux of some intermediate species (such as H atom) which diffuse outward from the flame zone. Over-prediction of these fluxes could lead to

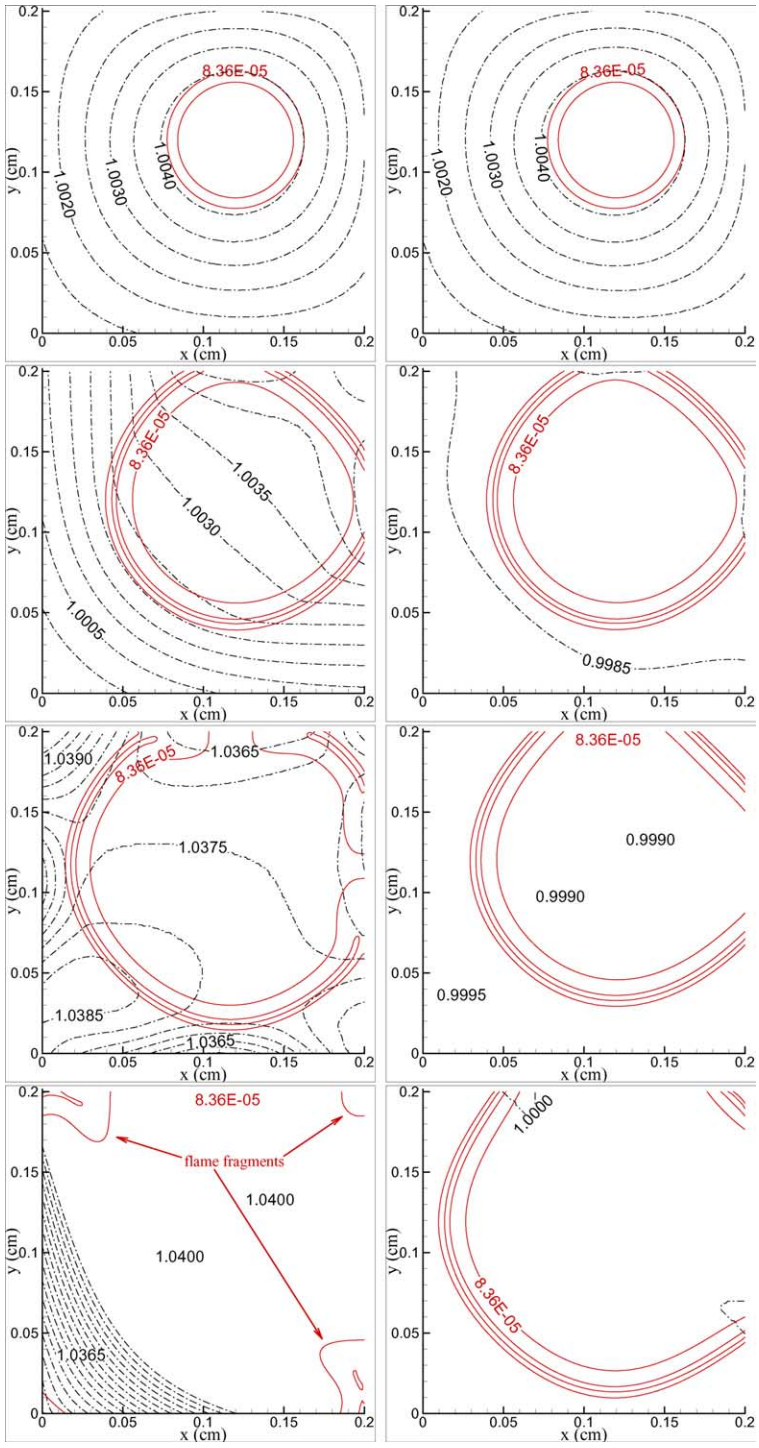

Fig. 5. Contours of pressure in atm (– · –) and mass fraction of HO_2 (–) for Case 3 at 10, 40, 55, and 85 μs. Pressure contour intervals are 5×10^{-4} atm. The figures at left use nonreflecting A; figures at right use nonreflecting B.

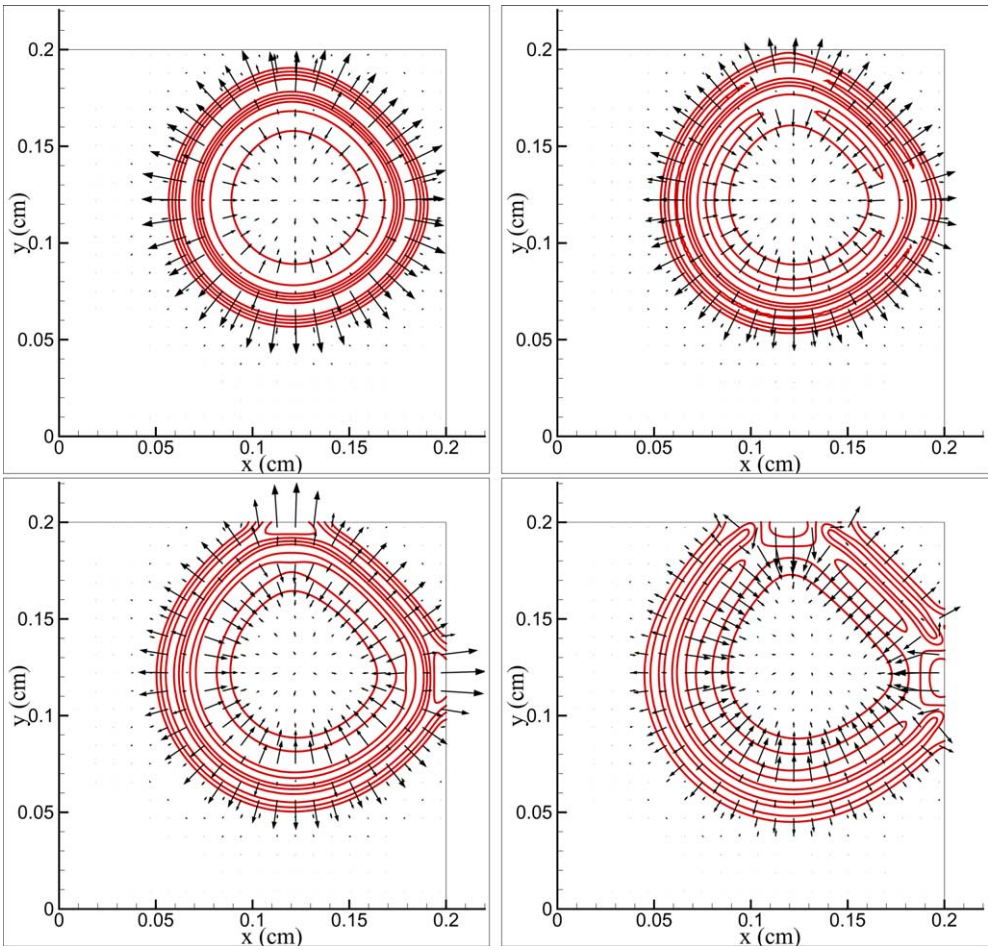

Fig. 6. Heat flux contours and vectors for Case 3 at 35, 40, 45, and 50 μs, showing the consequence of imposing zero flux gradients in the boundary-normal direction.

an artificially higher flame speed. It should be mentioned that specification of zero diffusive flux, $\mathbf{q} \cdot \mathbf{n} = 0$, $(\rho Y_i \mathbf{V}_i) \cdot \mathbf{n} = 0$, was unstable. This is not surprising, given that this would introduce strong discontinuities into the diffusive fluxes which, when differentiated, would produce very large terms in the governing equations. We have been unable to devise a more effective boundary condition for diffusive terms than zeroing flux gradients.

Figs. 5 and 6 show that the specification of zero flux gradients is not ideal, and leads to unphysical flame behavior at the boundary. However, the unified approach presented herein allows the flame to pass through the boundary with minimal effect on the interior of the domain. This capability is very useful, even if flame behavior at the boundary is not entirely physical.

5. Conclusions

This paper has focused on physical boundary condition theory and procedures for flame–boundary interactions of an ideal, multicomponent gas flow governed by the compressible NSE. The general form of

boundary conditions is considered from two somewhat different perspectives: those for incompletely parabolic systems and those for the hyperbolic Euler equations based on characteristic analysis. Using these, a rational mix of the two are used to specify inflow and outflow boundary conditions where nonreflection is often an objective. Unlike previous efforts at multicomponent flows, critical source terms containing body force and reaction rate terms are retained in the entire analysis. Accompanying these conditions is a clear procedure and tables outlining terms required for implementation in a multidimensional code. In the limits of zero reaction rate or one species, the boundary conditions reduce in a predictable way to the non-reacting and simple gas cases found in the literature. Application is then made to premixed and nonpremixed flames in one- and two-dimensions to establish efficacy.

With one exception, inclusion of source terms into the characteristic analysis provides greatly improved results relative to cases where source terms were neglected. For the cases considered, only pressure and species sources are nonzero. Inclusion of the pressure source term was uniformly beneficial. However, for nonreflecting inflow boundaries, we found that the source terms in the LODI relations for the species equations, s_{Y_i}, should be neglected. Simulations of both premixed and nonpremixed flames in one-dimension demonstrated that inclusion of source terms is essential to allow flames to pass through boundaries without significantly disturbing the interior solution. If source terms are neglected, large pressure gradients are generated, and flow reversals are observed as the flame encounters the nonreflecting boundary.

A two-dimensional simulation of a premixed flame propagating radially outward shows minor deficiencies in the boundary conditions, particularly in diffusive conditions associated with flames (heat flux and species diffusive flux). A slight acceleration of flames was observed as the boundary was approached. This is attributed to the boundary conditions on diffusive terms. There is some ambiguity in the literature as to the best form of the diffusive boundary conditions. Well-posedness favors specifying fluxes while experience suggests imposing boundary-normal flux derivatives. Vanishing diffusive fluxes give rise to severe flux discontinuities and do not work. Imposing vanishing boundary-normal gradients of the diffusive fluxes seems to be stable, but yields some unphysical behavior, such as slight flame acceleration near boundaries. More work is needed to address the optimal specification for diffusive boundary conditions, as well as multidimensional inviscid conditions.

Acknowledgements

The authors gratefully acknowledge the support of Sandia National Laboratories and DOE Basic Energy Sciences, Chemical Sciences Division. Sandia is a multiprogram laboratory operated by Sandia Corporation, a Lockheed Martin Company, for the United States Department of Energy under Contract DE-AC04-94-AL85000. We appreciate the assistance and support from Jacqueline H. Chen, Joseph C. Oefelein, Scott D. Mason, Hong G. Im, and Philip J. Smith.

Appendix A. Practical details for characteristic boundary treatments

Various results for characteristic boundary treatments require the **P** and **Q** matrices. Note that these are cast in terms of $N-1$ species because that is the way the equations are actually solved and that they are provided under the assumption of a Cartesian coordinate system. Furthermore, we assume that the conservative and primitive variables are given as $\mathbf{U} = \{\rho u, \rho v, \rho w, \rho, \rho e_0, \rho Y_i\}^{\mathrm{T}}$ and $\mathsf{U} = \{u, v, w, \rho, p, Y_i\}^{\mathrm{T}}$, respectively. Then, given the differential thermodynamic identity

$$\mathrm{d}e = -\frac{c_v T}{\rho}\mathrm{d}\rho + \frac{1}{\rho(\gamma-1)}\,\mathrm{d}p + \sum_{i=1}^{\mathrm{N}-1}(\mathfrak{h}_i - \mathfrak{h}_N)\,\mathrm{d}Y_i, \tag{A.1}$$

where $\mathfrak{h}_i = h_i - c_p TW/W_i$, we may compute $\mathbf{P} = \partial\mathbf{U}/\partial\mathsf{U}$ as

$$\begin{bmatrix} \rho & 0 & 0 & u & 0 & 0 & 0 & \cdots & 0 \\ 0 & \rho & 0 & v & 0 & 0 & 0 & \cdots & 0 \\ 0 & 0 & \rho & w & 0 & 0 & 0 & \cdots & 0 \\ 0 & 0 & 0 & 1 & 0 & 0 & 0 & \cdots & 0 \\ \rho u & \rho v & \rho w & e_0 - c_v T & \frac{1}{\gamma-1} & p_{5,6} & p_{5,7} & \cdots & p_{5,(5+N-1)} \\ 0 & 0 & 0 & Y_1 & 0 & \rho & 0 & \cdots & 0 \\ 0 & 0 & 0 & Y_2 & 0 & 0 & \rho & \cdots & 0 \\ \vdots & \vdots & \vdots & \vdots & \vdots & \vdots & \vdots & \ddots & \vdots \\ 0 & 0 & 0 & Y_{\mathrm{N}-1} & 0 & 0 & 0 & \cdots & \rho \end{bmatrix}, \tag{A.2}$$

with $p_{5,i} = \rho(\mathfrak{h}_i - \mathfrak{h}_N)$, $i = 6, 7, \ldots, N+4$. $\mathbf{Q} = \partial\mathbf{F}/\partial\mathsf{U}$ is then given by

$$\begin{bmatrix} \rho(u^{(\mathrm{n})} + u\delta_{1n}) & \rho u\delta_{2n} & \rho u\delta_{3n} & uu^{(\mathrm{n})} & \delta_{1n} & 0 & 0 & \cdots & 0 \\ \rho v\delta_{1n} & \rho(u^{(\mathrm{n})} + v\delta_{2n}) & \rho v\delta_{3n} & vu^{(\mathrm{n})} & \delta_{2n} & 0 & 0 & \cdots & 0 \\ \rho w\delta_{1n} & \rho w\delta_{2n} & \rho(u^{(\mathrm{n})} + w\delta_{3n}) & wu^{(\mathrm{n})} & \delta_{3n} & 0 & 0 & \cdots & 0 \\ \rho\delta_{1n} & \rho\delta_{2n} & \rho\delta_{3n} & u^{(\mathrm{n})} & 0 & 0 & 0 & \cdots & 0 \\ q_{5,1} & q_{5,2} & q_{5,3} & (e_0 - c_v T)u^{(\mathrm{n})} & \frac{\gamma u^{(\mathrm{n})}}{(\gamma-1)} & u^{(\mathrm{n})} p_{5,6} & u^{(\mathrm{n})} p_{5,7} & \cdots & u^{(\mathrm{n})} p_{5,(5+N-1)} \\ \rho Y_1\delta_{1n} & \rho Y_1\delta_{2n} & \rho Y_1\delta_{3n} & Y_1 u^{(\mathrm{n})} & 0 & \rho u^{(\mathrm{n})} & 0 & \cdots & 0 \\ \rho Y_2\delta_{1n} & \rho Y_2\delta_{2n} & \rho Y_2\delta_{3n} & Y_2 u^{(\mathrm{n})} & 0 & 0 & \rho u^{(\mathrm{n})} & \cdots & 0 \\ \vdots & \vdots & \vdots & \vdots & \vdots & \vdots & \vdots & \ddots & \vdots \\ \rho Y_{\mathrm{N}-1}\delta_{1n} & \rho Y_{\mathrm{N}-1}\delta_{2n} & \rho Y_{\mathrm{N}-1}\delta_{3n} & Y_{\mathrm{N}-1} u^{(\mathrm{n})} & 0 & 0 & 0 & \cdots & \rho u^{(\mathrm{n})} \end{bmatrix}, \tag{A.3}$$

where n is the boundary-normal direction, $u^{(\mathrm{n})} = \mathbf{u}\cdot\mathbf{n}$, $\delta_{\alpha n}$ is the Kronicker delta, and $q_{5,\alpha} = \rho\mathbf{u}_\alpha u^{(\mathrm{n})} + (\rho e_0 + p)\delta_{\alpha n}$, $\alpha = 1, 2, 3$. Multiplying the conservation form of the NSE by $\mathbf{P}^{-1}$, we obtain expressions for the source terms at the primitive variables level:

$$\begin{bmatrix} \mathsf{s}_u \\ \mathsf{s}_v \\ \mathsf{s}_w \\ \mathsf{s}_\rho \\ \mathsf{s}_p \\ \mathsf{s}_{Y_i} \end{bmatrix} = \begin{bmatrix} \sum_{i=1}^{N-1} Y_i(f_{ix} - f_{Nx}) + f_{Nx} \\ \sum_{i=1}^{N-1} Y_i(f_{iy} - f_{Ny}) + f_{Ny} \\ \sum_{i=1}^{N-1} Y_i(f_{iz} - f_{Nz}) + f_{Nz} \\ 0 \\ (1-\gamma)\sum_{i=1}^{N-1}[(\mathfrak{h}_i - \mathfrak{h}_N)W_i\dot{\omega}_i - \rho Y_i \mathbf{V}_{i\alpha}\cdot(\mathbf{f}_{i\alpha} - \mathbf{f}_{N\alpha})] \\ W_i\dot{\omega}_i/\rho \end{bmatrix}, \tag{A.4}$$

where $\mathbf{f}_{i\alpha}$ is the body force on species i in direction α. The components of the matrix $\mathsf{A} = \mathbf{P}^{-1}\mathbf{Q}$ in the boundary-normal direction are given by

$$\mathsf{A}^{(\mathrm{n})} = \begin{bmatrix} u^{(\mathrm{n})} & 0 & 0 & 0 & \frac{\delta_{1n}}{\rho} & 0 \\ 0 & u^{(\mathrm{n})} & 0 & 0 & \frac{\delta_{2n}}{\rho} & 0 \\ 0 & 0 & u^{(\mathrm{n})} & 0 & \frac{\delta_{3n}}{\rho} & 0 \\ \rho\delta_{1n} & \rho\delta_{2n} & \rho\delta_{3n} & u^{(\mathrm{n})} & 0 & 0 \\ \gamma p\delta_{1n} & \gamma p\delta_{2n} & \gamma p\delta_{3n} & 0 & u^{(\mathrm{n})} & 0 \\ 0 & 0 & 0 & 0 & 0 & u^{(\mathrm{n})}\delta_{ij} \end{bmatrix}. \tag{A.5}$$

In order to apply characteristic boundary treatments in all directions, several more results will be helpful. First, the eigenvalues of the $\mathsf{A}^{(\mathrm{n})}$ matrix, $\mathrm{diag}(\Lambda^{(\mathrm{n})}) = \lambda_\gamma^{(\mathrm{n})}$, are given by $\{\lambda_1^{(\mathrm{n})}, \lambda_2^{(\mathrm{n})}, \lambda_3^{(\mathrm{n})}, \lambda_4^{(\mathrm{n})}, \lambda_5^{(\mathrm{n})}, \lambda_{5+i}^{(\mathrm{n})}\} = \{(u^{(\mathrm{n})} - c),$

$u^{(n)}, u^{(n)}, u^{(n)}, (u^{(n)}+c), u^{(n)}\}$. With the eigenvalues, one may compute the associated right eigenvectors. These eigenvectors then form the columns of the $\mathsf{S}^{(n)}$ matrix. Next, the characteristic variables, $(\mathsf{S}^{(n)})^{-1}_{ad}\partial \mathsf{U}_d/\partial t$ and the sources at the characteristic level are given in Tables 3 and 4. The wave amplitude variations for each direction, $\mathscr{L} = \Lambda^{(n)}\mathsf{S}^{-1}(\nabla_{(n)}\mathsf{U})$, are given in Table 5. Inverting these relations, the boundary-normal gradient of the primitive variables is expressed in terms of the wave amplitude variations in Table 6. To generate boundary-normal gradient expressions for the conserved variables rather than the primitive variables we may write $(\mathbf{n}\cdot\nabla)\mathbf{U}_a = (\partial \mathbf{U}_a/\partial \mathsf{U}_b)(\mathbf{n}\cdot\nabla)\mathsf{U}_b = \mathbf{P}_{ab}(\mathbf{n}\cdot\nabla)\mathsf{U}_b$. For relations involving temperature or entropy, the differential relations expressed in terms of the primitive variables

$$\mathrm{d}T = \frac{T}{p}\,\mathrm{d}p - \frac{T}{\rho}\,\mathrm{d}\rho - TW\sum_{i=1}^{N}\frac{\mathrm{d}Y_i}{W_i}, \tag{A.6}$$

Table 3
Characteristic variables for each direction

$(\mathsf{S}^{(n)})^{-1}_{ad}\frac{\partial \mathsf{U}_d}{\partial t}$	x-Direction	y-Direction	z-Direction
$(\mathsf{S}^{(n)})^{-1}_{1d}\frac{\partial \mathsf{U}_d}{\partial t}$	$\frac{1}{2}\left(\frac{\partial p}{\partial t} - \rho c\frac{\partial u}{\partial t}\right)$	$\frac{1}{2}\left(\frac{\partial p}{\partial t} - \rho c\frac{\partial v}{\partial t}\right)$	$\frac{1}{2}\left(\frac{\partial p}{\partial t} - \rho c\frac{\partial w}{\partial t}\right)$
$(\mathsf{S}^{(n)})^{-1}_{2d}\frac{\partial \mathsf{U}_d}{\partial t}$	$\frac{-1}{c^2}\frac{\partial p}{\partial t} + \frac{\partial \rho}{\partial t}$	$\frac{-1}{c^2}\frac{\partial p}{\partial t} + \frac{\partial \rho}{\partial t}$	$\frac{-1}{c^2}\frac{\partial p}{\partial t} + \frac{\partial \rho}{\partial t}$
$(\mathsf{S}^{(n)})^{-1}_{3d}\frac{\partial \mathsf{U}_d}{\partial t}$	$\frac{\partial v}{\partial t}$	$\frac{\partial u}{\partial t}$	$\frac{\partial u}{\partial t}$
$(\mathsf{S}^{(n)})^{-1}_{4d}\frac{\partial \mathsf{U}_d}{\partial t}$	$\frac{\partial w}{\partial t}$	$\frac{\partial w}{\partial t}$	$\frac{\partial v}{\partial t}$
$(\mathsf{S}^{(n)})^{-1}_{5d}\frac{\partial \mathsf{U}_d}{\partial t}$	$\frac{1}{2}\left(\frac{\partial p}{\partial t} + \rho c\frac{\partial u}{\partial t}\right)$	$\frac{1}{2}\left(\frac{\partial p}{\partial t} + \rho c\frac{\partial v}{\partial t}\right)$	$\frac{1}{2}\left(\frac{\partial p}{\partial t} + \rho c\frac{\partial w}{\partial t}\right)$
$(\mathsf{S}^{(n)})^{-1}_{(5+i)d}\frac{\partial \mathsf{U}_d}{\partial t}$	$\frac{\partial Y_i}{\partial t}$	$\frac{\partial Y_i}{\partial t}$	$\frac{\partial Y_i}{\partial t}$

Table 4
Source terms at the characteristic level for each direction

s_a	x-Direction	y-Direction	z-Direction
s_1	$\frac{1}{2}(\mathsf{s}_p - \rho c\mathsf{s}_u)$	$\frac{1}{2}(\mathsf{s}_p - \rho c\mathsf{s}_v)$	$\frac{1}{2}(\mathsf{s}_p - \rho c\mathsf{s}_w)$
s_2	$\frac{-1}{c^2}\mathsf{s}_p$	$\frac{-1}{c^2}\mathsf{s}_p$	$\frac{-1}{c^2}\mathsf{s}_p$
s_3	s_v	s_u	s_u
s_4	s_w	s_w	s_v
s_5	$\frac{1}{2}(\mathsf{s}_p + \rho c\mathsf{s}_u)$	$\frac{1}{2}(\mathsf{s}_p + \rho c\mathsf{s}_v)$	$\frac{1}{2}(\mathsf{s}_p + \rho c\mathsf{s}_w)$
s_{5+i}	s_{Y_i}	s_{Y_i}	s_{Y_i}

Table 5
Characteristic wave amplitude variations for each direction

$\mathscr{L}_a$	x-Direction	y-Direction	z-Direction
$\mathscr{L}_1 =$	$\frac{(u-c)}{2}\left[\frac{\partial p}{\partial x} - \rho c \frac{\partial u}{\partial x}\right]$	$\frac{(v-c)}{2}\left[\frac{\partial p}{\partial y} - \rho c \frac{\partial v}{\partial y}\right]$	$\frac{(w-c)}{2}\left[\frac{\partial p}{\partial z} - \rho c \frac{\partial w}{\partial z}\right]$
$\mathscr{L}_2 =$	$\frac{u}{c^2}\left[c^2\frac{\partial \rho}{\partial x} - \frac{\partial p}{\partial x}\right]$	$\frac{v}{c^2}\left[c^2\frac{\partial \rho}{\partial y} - \frac{\partial p}{\partial y}\right]$	$\frac{w}{c^2}\left[c^2\frac{\partial \rho}{\partial z} - \frac{\partial p}{\partial z}\right]$
$\mathscr{L}_3 =$	$u\frac{\partial v}{\partial x}$	$v\frac{\partial u}{\partial y}$	$w\frac{\partial u}{\partial z}$
$\mathscr{L}_4 =$	$u\frac{\partial w}{\partial x}$	$v\frac{\partial w}{\partial y}$	$w\frac{\partial v}{\partial z}$
$\mathscr{L}_5 =$	$\frac{(u+c)}{2}\left[\frac{\partial p}{\partial x} + \rho c \frac{\partial u}{\partial x}\right]$	$\frac{(v+c)}{2}\left[\frac{\partial p}{\partial y} + \rho c \frac{\partial v}{\partial y}\right]$	$\frac{(w+c)}{2}\left[\frac{\partial p}{\partial z} + \rho c \frac{\partial w}{\partial z}\right]$
$\mathscr{L}_{5+i} =$	$u\frac{\partial Y_i}{\partial x}$	$v\frac{\partial Y_i}{\partial y}$	$w\frac{\partial Y_i}{\partial z}$.

$$\rho T\,\mathrm{d}s = \frac{1}{(\gamma-1)}\mathrm{d}p - c_p T\,\mathrm{d}\rho + \rho\sum_{i=1}^{N}\left(Ts_i - \frac{c_p TW}{W_i}\right)\mathrm{d}Y_i, \tag{A.7}$$

may be used in conjunction with $(\mathbf{n}\cdot\nabla)\mathsf{U}$ presented above by replacing d with $(\mathbf{n}\cdot\nabla)$. One may also relate source terms by replacing dx with s_x, not necessarily at the primitive variable level. The next step is to generate the $\mathsf{d}^{(\mathrm{n})}$ using $\mathsf{d}^{(\mathrm{n})} = \mathsf{S}^{(\mathrm{n})}\mathscr{L} = \mathsf{S}^{(\mathrm{n})}[\Lambda^{(\mathrm{n})}\mathsf{S}^{(n)\ -1}(\nabla_{(n)}\mathsf{U})] = \mathsf{A}^{(\mathrm{n})}_{bd}(\nabla_{(n)}\mathsf{U}_d)$, and c is the frozen speed of

Table 6
Boundary-normal gradients in terms of wave amplitude variations for each direction

$(\mathbf{n}\cdot\nabla)\mathsf{U}$	x-Direction	y-Direction	z-Direction
$(\mathbf{n}\cdot\nabla)u$	$\frac{1}{\rho c}\left(\frac{\mathscr{L}^{(x)}_5}{(u+c)} - \frac{\mathscr{L}^{(x)}_1}{(u-c)}\right)$	$\frac{\mathscr{L}^{(y)}_3}{v}$	$\frac{\mathscr{L}^{(z)}_3}{w}$
$(\mathbf{n}\cdot\nabla)v$	$\frac{\mathscr{L}^{(x)}_3}{u}$	$\frac{1}{\rho c}\left(\frac{\mathscr{L}^{(y)}_5}{(v+c)} - \frac{\mathscr{L}^{(y)}_1}{(v-c)}\right)$	$\frac{\mathscr{L}^{(z)}_4}{w}$
$(\mathbf{n}\cdot\nabla)w$	$\frac{\mathscr{L}^{(x)}_4}{u}$	$\frac{\mathscr{L}^{(y)}_4}{v}$	$\frac{1}{\rho c}\left(\frac{\mathscr{L}^{(z)}_5}{(w+c)} - \frac{\mathscr{L}^{(z)}_1}{(w-c)}\right)$
$(\mathbf{n}\cdot\nabla)\rho$	$\frac{\mathscr{L}^{(x)}_2}{u} + \frac{1}{c^2}\left(\frac{\mathscr{L}^{(x)}_5}{(u+c)} + \frac{\mathscr{L}^{(x)}_1}{(u-c)}\right)$	$\frac{\mathscr{L}^{(y)}_2}{v} + \frac{1}{c^2}\left(\frac{\mathscr{L}^{(y)}_5}{(v+c)} + \frac{\mathscr{L}^{(y)}_1}{(v-c)}\right)$	$\frac{\mathscr{L}^{(z)}_2}{w} + \frac{1}{c^2}\left(\frac{\mathscr{L}^{(z)}_5}{(w+c)} + \frac{\mathscr{L}^{(z)}_1}{(w-c)}\right)$
$(\mathbf{n}\cdot\nabla)p$	$\left(\frac{\mathscr{L}^{(x)}_5}{(u+c)} + \frac{\mathscr{L}^{(x)}_1}{(u-c)}\right)$	$\left(\frac{\mathscr{L}^{(y)}_5}{(v+c)} + \frac{\mathscr{L}^{(y)}_1}{(v-c)}\right)$	$\left(\frac{\mathscr{L}^{(z)}_5}{(w+c)} + \frac{\mathscr{L}^{(z)}_1}{(w-c)}\right)$
$(\mathbf{n}\cdot\nabla)Y_i$	$\frac{\mathscr{L}^{(x)}_{5+i}}{u}$	$\frac{\mathscr{L}^{(y)}_{5+i}}{v}$	$\frac{\mathscr{L}^{(z)}_{5+i}}{w}$

Table 7
$\mathsf{d}^{(\mathrm{n})}$ as a function of wave amplitude variations for the each direction

d_b	$\mathsf{d}^{(x)} = \mathsf{A}^{(x)}(\nabla_{(x)}\mathsf{U})$	$\mathsf{d}^{(y)} = \mathsf{A}^{(y)}(\nabla_{(y)}\mathsf{U})$	$\mathsf{d}^{(z)} = \mathsf{A}^{(z)}(\nabla_{(z)}\mathsf{U})$
$\mathsf{d}_1 =$	$\frac{1}{c^2}\left[c^2\mathscr{L}_2^{(x)} + \left(\mathscr{L}_5^{(x)} + \mathscr{L}_1^{(x)}\right)\right]$	$\frac{1}{c^2}\left[c^2\mathscr{L}_2^{(y)} + \left(\mathscr{L}_5^{(y)} + \mathscr{L}_1^{(y)}\right)\right]$	$\frac{1}{c^2}\left[c^2\mathscr{L}_2^{(z)} + \left(\mathscr{L}_5^{(z)} + \mathscr{L}_1^{(z)}\right)\right]$
$\mathsf{d}_2 =$	$\left(\mathscr{L}_5^{(x)} + \mathscr{L}_1^{(x)}\right)$	$\left(\mathscr{L}_5^{(y)} + \mathscr{L}_1^{(y)}\right)$	$\left(\mathscr{L}_5^{(z)} + \mathscr{L}_1^{(z)}\right)$
$\mathsf{d}_3 =$	$\frac{1}{\rho c}\left(\mathscr{L}_5^{(x)} - \mathscr{L}_1^{(x)}\right)$	$\mathscr{L}_3^{(y)}$	$\mathscr{L}_3^{(z)}$
$\mathsf{d}_4 =$	$\mathscr{L}_3^{(x)}$	$\frac{1}{\rho c}\left(\mathscr{L}_5^{(y)} - \mathscr{L}_1^{(y)}\right)$	$\mathscr{L}_4^{(z)}$
$\mathsf{d}_5 =$	$\mathscr{L}_4^{(x)}$	$\mathscr{L}_4^{(y)}$	$\frac{1}{\rho c}\left(\mathscr{L}_5^{(z)} - \mathscr{L}_1^{(z)}\right)$
$\mathsf{d}_{5+i} =$	$\mathscr{L}_{5+i}^{(x)}$	$\mathscr{L}_{5+i}^{(y)}$	$\mathscr{L}_{5+i}^{(z)}$

Table 8
Boundary-normal convection term, $\nabla_{(n)} \cdot \mathbf{F}^{(\mathrm{n})}$, for each direction

Equation	$\nabla_{(n)} \cdot \mathbf{F}^{(\mathrm{n})} = \mathbf{P}\mathsf{S}^{(\mathrm{n})}\mathscr{L}^{(\mathrm{n})}$
Continuity	$\mathsf{d}_1^{(\mathrm{n})}$
x-Momentum	$u\mathsf{d}_1^{(\mathrm{n})} + \rho\mathsf{d}_3^{(\mathrm{n})}$
y-Momentum	$v\mathsf{d}_1^{(\mathrm{n})} + \rho\mathsf{d}_4^{(\mathrm{n})}$
z-Momentum	$w\mathsf{d}_1^{(\mathrm{n})} + \rho\mathsf{d}_5^{(\mathrm{n})}$
Energy	$\rho u\mathsf{d}_3^{(\mathrm{n})} + \rho v\mathsf{d}_4^{(\mathrm{n})} + \rho w\mathsf{d}_5^{(\mathrm{n})} + \sum_{i=1}^{N-1}\rho\mathsf{d}_{5+i}^{(\mathrm{n})}(\mathsf{h}_i - \mathsf{h}_N) + (e_0 - c_v T)\mathsf{d}_1^{(\mathrm{n})} + \frac{\mathsf{d}_2^{(\mathrm{n})}}{(\gamma-1)}$
i-Species	$Y_i\mathsf{d}_1^{(\mathrm{n})} + \rho\mathsf{d}_{5+i}^{(\mathrm{n})}$

sound. These are listed in Table 7. Finally, the boundary-normal convection term $\nabla_{(n)} \cdot \mathbf{F}^{(\mathrm{n})} = \mathbf{P}\mathsf{S}^{(\mathrm{n})}\mathscr{L}^{(\mathrm{n})}$ is given in Table 8. To impose boundary conditions based on the time variation of the primitive or conservation variables, one may use $(\partial \mathsf{U}_b/\partial t) = \mathsf{s}_b - \mathsf{d}_b^{(\mathrm{n})}$ to find $(\partial \mathbf{U}_a/\partial t) = \mathbf{P}_{ab}(\partial \mathsf{U}_b/\partial t) = \mathbf{P}_{ab}(\mathsf{s}_b - \mathsf{d}_b^{(\mathrm{n})})$. If relations for temperature or entropy are needed, the thermodynamic relations (A.7) should be used.

References

[1] R. Hixon, S.H. Shih, R.R. Mankbadi, Evaluation of boundary conditions for computational aeroacoustics, AIAA J. 33 (11) (1995) 2006–2012.
[2] C.K.W. Tam, Advances in numerical boundary conditions for computational aeroacoustics, J. Comp. Acoust. 6 (4) (1998) 377–402.
[3] F. Nicoud, Defining wave amplitude in characteristic boundary conditions, J. Comp. Phys. 149 (2) (1999) 418–422.
[4] C.W. Rowley, T. Colonius, Discretely nonreflecting boundary conditions for linear hyperbolic systems, J. Comp. Phys. 157 (2) (2000) 500–538.

[5] B. Gustafsson, A. Sundström, Incompletely parabolic problems in fluid-dynamics, SIAM J. Appl. Math. 35 (2) (1978) 343–357.
[6] J. Oliger, A. Sundström, Theoretical and practical aspects of some initial boundary-value problems in fluid-dynamics, SIAM J. Appl. Math. 35 (3) (1978) 419–446.
[7] P. Dutt, Stable boundary conditions and difference schemes for Navier–Stokes equations, SIAM J. Numer. Anal. 25 (2) (1988) 245–267.
[8] J.S. Hesthaven, D. Gottlieb, A stable penalty method for the compressible Navier–Stokes equations. I. Open boundary conditions, SIAM J. Sci. Comp. 17 (3) (1996) 579–612.
[9] D. Michelson, Initial-boundary value problems for incomplete singular perturbations of hyperbolic systems, J. D'analyse Mathèmatique 53 (1989) 1–138.
[10] T.J. Poinsot, S.K. Lele, Boundary conditions for direct simulations of compressible viscous flows, J. Comp. Phys. 101 (1) (1992) 104–139.
[11] T. Poinsot, D. Veynante, Theoretical and Numerical Combustion, R.T. Edwards Inc, Philadelphia, 2001.
[12] K.W. Thompson, Time-dependent boundary conditions for hyperbolic systems, J. Comp. Phys. 68 (1) (1987) 1–24.
[13] F.F. Grinstein, Open boundary conditions in the simulation of subsonic turbulent shear flows, J. Comp. Phys. 115 (1) (1994) 43–55.
[14] M. Baum, T.J. Poinsot, D. Thévenin, Accurate boundary conditions for multicomponent reactive flows, J. Comp. Phys. 116 (2) (1995) 247–261.
[15] D. Thévenin, M. Baum, T.J. Poinsot, Description of accurate boundary conditions for the simulation of reactive flows, in: T. Baritaud, T. Poinsot, M. Baum (Eds.), Direct Numerical Simulation for Turbulent Reacting Flows, Éditions Technip, Paris, 1996, pp. 12–32.
[16] L. Jiang, H. Shan, C. Liu, M.R. Visbal, Non-reflecting boundary conditions for DNS in curvilinear coordinates, in: D. Knight, L. Sakell (Eds.), Recent Advances in DNS and LES, Kluwer Academic Publishers, Dordrecht, 1999, pp. 219–233.
[17] K.E. Rian, Open boundaries and non-reflecting boundary conditions, Technical Report TR-A5048, SINTEF Energy Res., Trondheim, 1999.
[18] R. Prosser, Toward improving boundary conditions for reactive flow simulations I: acoustically transparent inflow boundary conditions, J. Comp. Phys. (2002) (submitted).
[19] N. Okong'o, J. Bellan, Consistent boundary conditions for multicomponent real gas mixtures based on characteristic waves, J. Comp. Phys. 176 (2) (2002) 330–344.
[20] J.C. Strikwerda, Initial boundary-value problems for incompletely parabolic systems, Commun. Pure Appl. Math. 9 (3) (1977) 797–822.
[21] L. Halpern, Artificial boundary conditions for incompletely parabolic perturbations of hyperbolic systems, SIAM J. Math. Anal. 22 (5) (1991) 1256–1283.
[22] G. Lill, Exact and approximate boundary conditions at artificial boundaries, Math. Meth. Appl. Sci. 16 (10) (1993) 691–705.
[23] P. Caussignac, Incompletely parabolic systems from Friedrichs theory point of view, Math. Models Meth. Appl. Sci. 7 (8) (1997) 1141–1152.
[24] D. Michelson, Initial-boundary value problems for incomplete singular perturbations of hyperbolic systems, in: B. Engquist, S. Osher, R. Somerville (Eds.), Large-scale Computations in Fluid Mechanics, Part 2 of Lectures in Applied Mathematics, vol. 22, AMS, Providence, 1985, pp. 127–132.
[25] L. Tourrette, Artificial boundary conditions for the linearized compressible Navier–Stokes equations, J. Comp. Phys. 137 (1) (1997) 1–37.
[26] D. Gottlieb, M. Gunzburger, E. Turkel, On numerical boundary treatment of hyperbolic systems for finite difference and finite element methods, SIAM J. Numer. Anal. 19 (4) (1982) 671–682.
[27] G.W. Hedstrom, Nonreflecting boundary conditions for non-linear hyperbolic systems, J. Comp. Phys. 30 (2) (1979) 222–237.
[28] B. Gustafsson, J. Nordström, Extrapolation procedures at outflow boundaries for the Navier–Stokes equations, in: R. Glowinsky, A. Lichnewsky (Eds.), Computing Methods in Applied Sciences and Engineering, SIAM, Philadelphia, 1990, pp. 136–151.
[29] J. Nordström, On flux-extrapolation at supersonic outflow boundaries, Appl. Numer. Math. 30 (4) (1999) 447–457.
[30] J. Nordström, Accurate solutions of the Navier–Stokes equations despite unknown outflow boundary data, J. Comp. Phys. 120 (2) (1995) 184–205.
[31] J. Nordström, The use of characteristic boundary conditions for the Navier–Stokes equations, Comp. Fluids 24 (5) (1995) 609–623.
[32] D.H. Rudy, J.C. Strikwerda, A nonreflecting outflow boundary-condition for subsonic Navier–Stokes calculations, J. Comp. Phys. 36 (1) (1980) 55–70.
[33] F.A. Williams, Combustion Theory, second ed., Benjamin/Cummings, Menlo Park, 1985.
[34] R.J. Kee, G. Dixon-Lewis, J. Warnatz, M.E. Coltrin, J.A. Miller, H.K. Moffat, Transport, Reaction Design Inc., San Diego, CA, release 3.5, 1999.
[35] R.A. Yetter, F.L. Dryer, H. Rabitz, A comprehensive reaction mechanism for carbon-monoxide hydrogen oxygen kinetics, Combust. Sci. Technol. 79 (1-3) (1991) 97–128.

[36] C.A. Kennedy, M.H. Carpenter, A comparison of several new numerical methods for the simulation of compressible shear layers, Appl. Numer. Math. 14 (4) (1994) 397–433.
[37] C.A. Kennedy, M.H. Carpenter, R.H. Lewis, Low-storage, explicit Runge–Kutta schemes for the compressible Navier–Stokes equations, Appl. Numer. Math. 35 (3) (2000) 177–219.